Quantification of the Attenuation of Storm Surge Components by a Coastal Wetland of the US Mid Atlantic

Anne-Eleonore Paquier[1] · Jana Haddad[1] · Seth Lawler[1] · Celso M. Ferreira[1]

Abstract Coastal wetlands are receiving increased consideration as natural defenses for coastal communities from storm surge. However, there are gaps in storm surge measurements collected in marsh areas during extreme events as well as understanding of storm surge processes. The present study evaluates the importance and variation of different processes (i.e., wave, current, and water level dynamics with respect of the marsh topography and vegetation characteristics) involved in a storm surge over a marsh, assesses how these processes contribute to storm surge attenuation, and quantifies the storm surge attenuation in field conditions. During the Fall of 2015, morphology and vegetation surveys were conducted along a marsh transect in a coastal marsh located at the mouth of the Chesapeake Bay, mainly composed of *Spartina alterniflora* and *Spartina patens*. Hydrodynamic surveys were conducted during two storm events. Collected data included wave characteristics, current velocity and direction, and water levels. Data analysis focused on the understanding of the cross-shore evolution of waves, currents and water level, and their influence on the overall storm surge attenuation. Results indicate that the marsh area, despite its short length, attenuates waves and reduces current velocity and water level. Tides have a dominant influence on current direction and velocity, but the presence of vegetation and the marsh morphology contribute to a strong reduction of current velocity over the marsh platform relative to the currents at the marsh front. Wave attenuation varies across the tide cycle which implies a link between wave attenuation and water level and, consequently, storm surge height. Storm surge reduction, here assessed through high water level (HWL) attenuation, is linked to wave attenuation across the front edge of the marsh; this positive trend highlights the reduction of water level height induced by wave setup reduction during wave propagation across the marsh front edge. Water level attenuation rates observed here have a greater range than the rates observed or modeled by other authors, and our results suggest that this is linked to the strong influence of waves in storm surge attenuation over coastal areas.

Keywords Storm surge attenuation · Water level · Waves · Currents · Coastal wetland · Nature-based defenses

Introduction

Tropical cyclones are one of the most costly natural hazards in the United States (Lott and Ross 2006), and examples in recent history, such as Katrina (2005), Ike (2008), or Sandy (2012), demonstrate the magnitude of infrastructure losses and societal impacts in some of the most developed regions of the country. Salt marshes, besides their well-documented ecological functions (Lavoie et al. 2016; Xue et al. 2008), have gained increased recognition as nature-based strategies for reducing the risks faced by coastal communities from sea level rise and coastal storms (Arkema et al. 2013; Spalding et al. 2014b). The move toward integrating green infrastructure as a component of coastal resiliency efforts has gained traction at the highest levels in the United States. For instance, the US Executive Office of the President (National Science

✉ Anne-Eleonore Paquier
   eleonorepaquier@gmail.com

1 Civil, Environmental and Infrastructure Engineering, Volgenau School of Engineering, Department of Civil, Environmental and Infrastructure Engineering, George Mason University, 4400 University Drive, MS 6C1, Nguyen Engineering Bldg, Fairfax, VA 22030, USA

and Technology Council) has recently published a report highlighting the research needs for coastal green infrastructure (Committee on Environment, Natural, Resources, and Sustainability, National Science and Technology Council 2015) and the United States Army Corps of Engineers (USACE) included the use of Natural and Nature Based Features (NNBF) in its risk management strategies for coastal communities (Bridges et al. 2015).

The scientific community has been working on the interactions of coastal vegetation and hydrodynamics for decades. That body of research supports the idea that coastal vegetation, including wetlands and coastal marshes, has the potential to act as a resilient defense system against the risks of flooding and erosion. Several recent comprehensive reviews have highlighted the ability of salt marshes to protect and stabilize shorelines and the contribution of salt marsh vegetation in wave attenuation (Gedan et al. 2011; Shepard et al. 2011; Spalding et al. 2014a; Sutton-Grier et al. 2015). Several studies have investigated and demonstrated the ability of marsh vegetation to attenuate waves (Anderson and Smith 2014; John et al. 2015; Marsooli and Wu 2014) including laboratory studies under storm surge conditions (Möller et al. 2014) but much fewer based on field experiments (Coulombier et al. 2012; Tschirky et al. 2001). It has been demonstrated that this attenuation can vary as a function of wave conditions and water level (Marsooli and Wu 2014; Möller et al. 2014) but is also dependent on plant biometric characteristics (Coulombier et al. 2012) such as stem stiffness (Bouma et al. 2005), stem density, or submergence ratio (Anderson and Smith 2014). It has also been demonstrated through laboratory experiments that vegetation with characteristics of a typical marsh ecosystem reduces current velocity (Leonard et al. 1995; Nepf 1999; Neumeier 2007; Neumeier and Ciavola 2004; Leonard and Croft 2006; Peralta et al. 2008).

Several numerical modeling studies have also investigated the role of wetlands in storm surge attenuation. Numerical studies have identified and tested the role of morphological parameters. For example, Loder et al. (2009) found that marsh discontinuity (defined by the presence of streams) increases storm surge height while Wamsley et al. (2010) found that the presence of more complex bed forms decrease it. Sheng et al. (2012) highlighted the importance of vegetation characteristics on bottom friction and consequently on storm surge attenuation. It has been demonstrated that the attenuation of storm surge by wetlands is also highly dependent on the hydrodynamic process of storm surge and the unique meteorological characteristics of storms (Loder et al. 2009; Resio and Westerink 2008; Wamsley et al. 2010). Authors have proposed storm surge attenuation rates from 4 to 25 cm.km^{-1} over marshes and mangroves during Hurricanes Andrew in 1992 (Lovelace 1994), Charley in 2004, Wilma in 2005 (Krauss et al. 2009), and Rita in 2005 (McGee et al. 2005).

Attenuation rates from −2 to 70 cm.km^{-1} over tides— undermarsh tides, overmarsh tides, and storm tides—have also been proposed during moderate and severe storms (Stark et al. 2015). These results, reviewed by Stark et al. (2015), to the best of our knowledge, document the majority of field surveys available to evaluate attenuation of storm surge over wetlands. Therefore, there remains a significant need for storm surge measurements collected in marsh areas during extreme events (Bouma et al. 2014; Thomas et al. 2014), particularly in the US Mid-Atlantic region (Hu et al. 2015; Shepard et al. 2011).

While most of the studies have tried to resolve the question of storm surge attenuation over wetlands using a modeling approach, this study focuses on field experiments. The aim here is to reduce the existing knowledge gap by acquiring high resolution field data and analyzing the non-linear interactions of hydrodynamics, bed morphology, and vegetation characteristics in a coastal marsh for two coastal storms. We thus have collected and present here a field dataset composed of high-resolution measurements of bed morphology, vegetation characteristics, and hydrodynamics (wave, current velocity, current direction, and water level). Our goals are to broaden the understanding of hydrodynamics in marsh areas and to determine how and to what extent these natural areas effectively attenuate surges. The hydrodynamics (waves, current velocity and direction, and water levels) were observed during two storm events within a coastal wetland located at the mouth of the Chesapeake Bay to provide a basis for resolving the key questions involving the importance and variation of processes composing a storm surge, how these processes contribute to attenuation of a storm surge, and the quantification of storm surge attenuation over a marsh area during storm events.

Methods

Study Area and Study Site

The Chesapeake Bay is the largest estuary in the US and is located on the Mid-Atlantic coast (Fig. 1a). The study site is located at the Eastern Shore of Virginia National Wildlife Refuge (ESVNWR) managed by the US Fish and Wildlife Service (USFWS) on the Southern end of the Eastern Shore of the Chesapeake Bay, on the Delmarva Peninsula (Fig. 1c). The tidal amplitudes are observed at the National Oceanic and Atmospheric Administration (NOAA) s Chesapeake Bay Bridge Tunnel (CBBT) station (Fig. 1c) with a mean range of tide of 0.77 m. Wind measurements at CBBT during 2015 (Fig. 1b) show that North winds (WNW to NE) and South-Southwest winds (S to SW) are the most prevalent.

The coastal marsh area which encompasses the ESVNWR lies on the ocean side of the Eastern Shore of the Chesapeake Bay (Fig. 2a). The coastal marsh is located in a fetch-limited
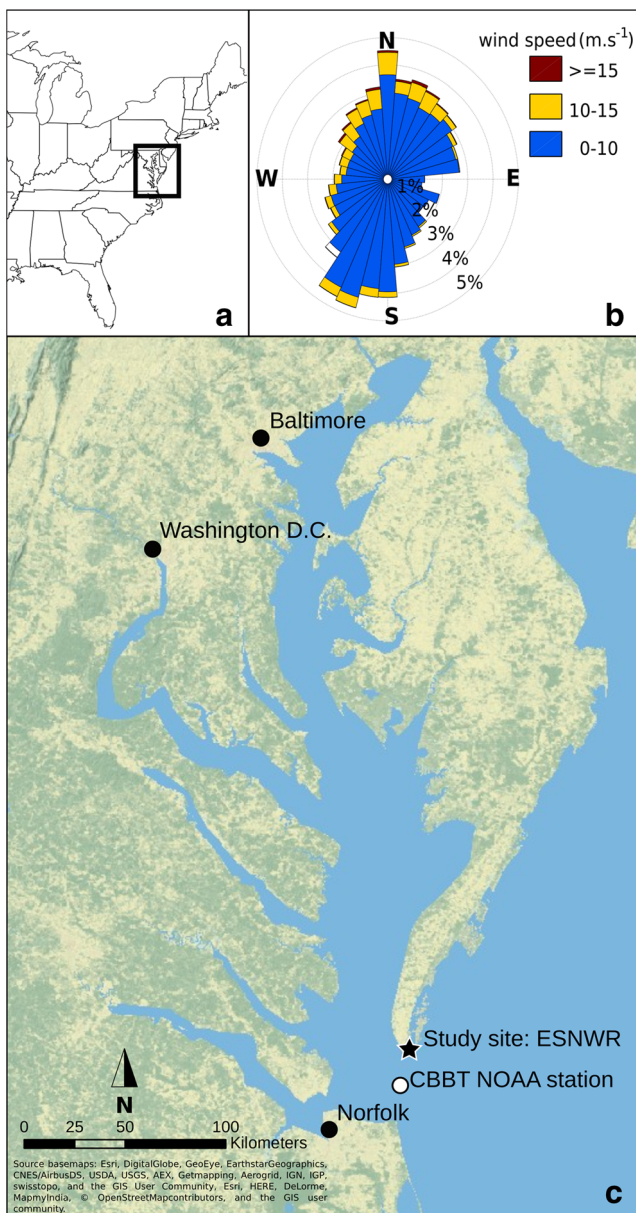
Fig. 1 Study area. **a** Location in the United States. **b** Wind rose presenting the wind data collected from 2015/01/01 to 2015/12/02 at Chesapeake Bay Bridge Tunnel (CBBT) NOAA Station. **c** Chesapeake Bay, location of the study site (marked by a *black star*), location of the CBBT NOAA station (marked by a *white circle*)

extreme events. The marsh is bordered by a forest further to the West and North. As is the case for much of the Chesapeake Bay region's coastal marshes (Knutson et al. 1982; Perry et al. 2001), the dominant species of vegetation is *Spartina alterniflora* in the lower marsh and *Spartina patens* in the upper marsh. *Distichlis spicata* and *Phragmites australis* are also present on the highest points bordering the forested areas.

The site, a natural setting highly exposed to tidal and surge inundation, gives an opportunity to examine the impact on storm-induced waves, currents, and water levels by a marsh with vegetation typical for the Mid-Atlantic region. Measurements of waves, current direction and velocity, and water level were taken along a 500-m-long cross-shore transect for two successive storm events, from the 24th of September 2015 to the 26th of October 2015. Figure 2b shows the placements of instruments on this transect, with "W" representing wave measurements, "AQP" representing the current measurements, "WL" representing water level, and green dots representing the vegetation measurements. This transect was also characterized in terms of topography and vegetation characteristics. While water levels and currents were monitored throughout the period of survey, waves were monitored only during the first event. Though tide ranges were measured on site, the wind and tide records at CBBT (located at the mouth of the bay) were used as proxies to characterize these storms.

Environmental Context

Topography

A high-resolution topographic survey was performed on the marsh area and the submerged beach using a differential GPS Trimble R4 (error lower than 0.02 m in elevation). Cross-shore and long-shore transects spaced at 15 to 30 m were recorded by walking surveys using the rover GPS fixed on a backpack. The error associated with the instrument is here increased as a result of the surveyor and the backpack movement; to account for thus additional uncertainty, we increased the final vertical error to 0.1 m. The point sampling density was increased for significant features, such as bottom and top of marsh front edge and significant streams. The transect topography was surveyed using 1-s measurements with the rover GPS mounted to a pole. Measurements are geo-referenced to the NAVD88 vertical datum and NAD83 horizontal datum for easting and northing locations. The location of the GPS base was corrected using the Online Positioning User Service of the National Geodetic Survey (NOAA-NGS). From the corrected data, a 1 m-cell digital elevation model (DEM) was computed using a Delaunay triangulation method (Fig. 2b).

area delimited by discontinuous barrier islands. The inlet fronting the reserve allows the propagation of waves from the southeast and currents from the open sea. The study site is a wetland located within ESVNWR (Fig. 2b). It has a steep front edge, a relatively flat topography, and is cut by a roughly 0.8 m deep and 5 m wide stream diverting into two shallow tributaries as the depth of the main branch decreases further inland. These streams occupy the lower marsh platform which has elevations around mean sea level (MSL). The inland most part of the wetland (upper marsh) shows a more significant slope and is inundated only during particularly high tides or

Fig. 2 Study site, Eastern Shore National Wildlife Refuge (ESVNWR). **a** Location of ESVNWR at the southernmost end of the Delmarva Peninsula, marked by a *black star*. **b** Study site. Map showing the DEM carried out in the wetland and the location of the instruments deployed during the Fall 2015. AQP1 and AQP2 (*purple squares*) are Acoustic Doppler Current profilers used for current direction and velocity measurements, WL1 to WL5 (*light blue dots*) are low frequency pressure sensors used for water level measurements and W1 to W4 (*dark blue stars*) are high frequency pressure sensors used for measurements of wave parameters. *Green dots* represent the location of the vegetation measurement stations
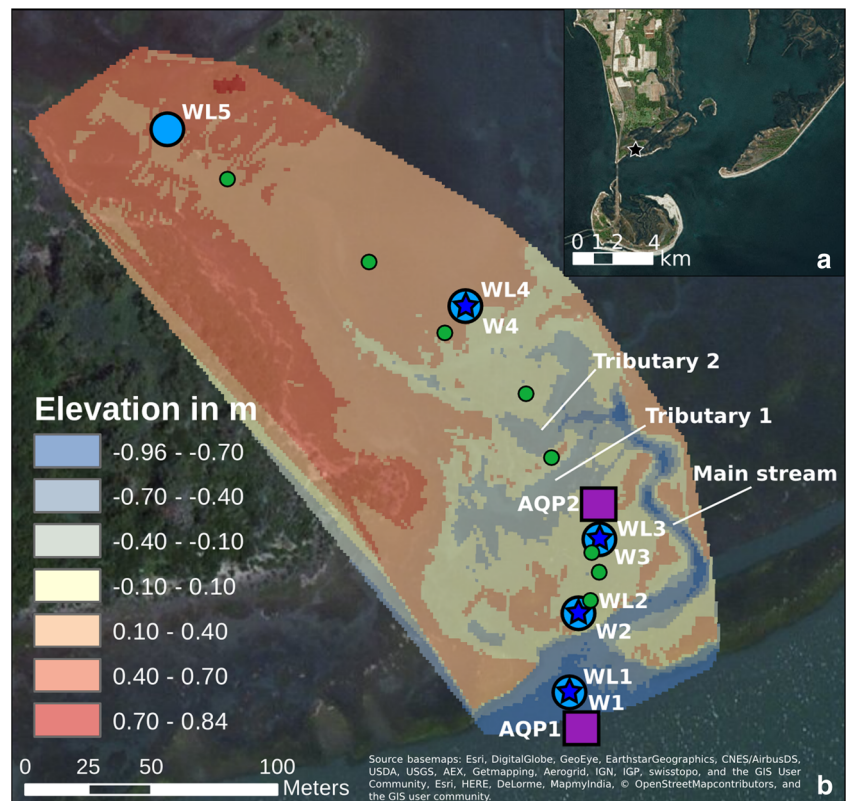
Vegetation

On the 17th of October 2015, a non-destructive vegetation survey was performed along the surveyed transect. Vegetation biometry was measured at three stations between WL2 and WL3, two stations between WL3 and WL4, and three stations between WL4 and WL5. At each station, photos were taken to perform species recognition, and the stem density was counted in three quadrats of 25 cm^2. In each quadrat, five plant heights and stem diameters were also measured. For each station, mean values were computed for stem density (per m^2), plant height (cm), and stem diameter (mm). The variability associated with the measurements was evaluated by standard deviations. The locations of the vegetation survey quadrats were surveyed precisely using 1-s points with the pole mounted rover GPS.

Hydrodynamics

Waves

Four high-frequency pressure transducers (Trublue Measurement Specialties) were deployed along the transect on wood posts and are identified as W1, W2, W3, and W4 (Fig. 2b). The accuracy of the sensor is 0.05 % of the instrument full scale (0–50 psi) being 0.01 m in the present study.

The locations of these sensors were surveyed by Differential GPS (3-min point measurements). These sensors recorded continuously at 4 Hz. The time series was cut in bursts of 4800 sample measurements (20 min) on which wave spectra were calculated using Fast Fourier Transforms and a 600 s Hanning window with 75 % overlapping (Sénéchal et al. 2001). The limit between the gravity and infra-gravity was set at 0.06 Hz. As proposed by Horikawa (1988), a correction factor was applied to account for the non-hydrostatic pressure field. This induced a 0.5 Hz cut-off. For each burst, significant wave height (H_s) and peak period (T_p) were calculated in the spectral window [0.06; 0.5] Hz. Several studies characterized wave attenuation by an exponential decay process (Anderson and Smith 2014; Coulombier et al. 2012; Jadhav and Chen 2012; Möller et al. 1999) expressed as follows:

$$H = H_0 e^{-K_i x}$$

where H_0 is the wave height at the first station, H the wave height at the second station, x the distance between the stations, and K_i the wave height decay rate.

For this study, we limited our consideration to waves exceeding 0.05 m. Also, even if wind waves are expected in this fetch-limited area, wind measurements were outside the scope of this study. Moreover, in this area, swell is propagated from the Atlantic Ocean through the inlet fronting the site. We thus expected swell to be the dominant wave dynamic.

Current Velocity and Direction

Two Acoustic Doppler Current Profilers (ADCPs), Aquadopp Nortek 2 MHz, were deployed during both storm events and geo-referenced by Differential GPS. These instruments have an accuracy of 0.01 % of the measured value for current velocity (maximum of 8×10^{-5} m.s^{-1} in the present study) and 0.2° for current direction. One was deployed in the water (station AQP1) and the other in the marsh (station AQP2), as shown in Fig. 2b. The ADCPs were installed in up-looking position on microfiber gridded structures fixed to the bed. They were both configured to collect current velocity and direction on 10 cm bins, with a 0.1 m blanking distance, to obtain 1-min-averaged profiles every 10 min.

Water Levels

Five low-frequency pressure transducers (Hobo Onset U20L-01) were continuously deployed a few centimeters from the bed on the same posts used for wave measurements: WL1 to WL5 as shown in Fig. 2b. The accuracy of these sensors is evaluated at 0.02 m by the manufacturer. Atmospheric pressure was measured using the same instruments at a nearby location. These sensors measured instantaneous pressure every 6 min, which was corrected from atmospheric pressure and converted to water levels above NAVD88. The observed instantaneous water levels were scattered, and the spread was particularly significant at WL1 and decreased along the transect. Wave dynamics can increase the instantaneous water level via passing of a wave crest or wave set-up and can decrease it via passing of a wave trough or wave breaking. These water level variations observed shore-ward can be a source of uncertainty which has been evaluated by calculation of standard deviations on moving averages (averaged on 5 values). The sum of the uncertainties for two stations was consistently lower than the average of absolute differences of water level between the same stations. The uncertainties in water level gradients were evaluated as 0.19, 0.09, 0.02, and 0.01 cm.m^{-1} for each section from WL1 to WL5, and 0.01 cm.m^{-1} over the entire marsh platform (WL2 to WL5). Considering that we analyzed the general pattern of the observed water surface slopes over the studied period (as described below) and that these uncertainties were lower than the values of water level gradients, we considered these results valid. On the other hand, the variability of water level signals (due to the passing of wave crest and trough, wave breaking, and wave setup) can be used, on top of wave data, as an element of interpretation of the implication of wave dynamics on the water level variation.

The comparison of water level values along a cross-shore transect for the evaluation of water surface slope or high water level attenuation requires that storm surge direction is parallel to the surveyed transect. Current measurements showed that the current direction in the main part of the water column at the entrance of the marsh was parallel to the surveyed transect during the low energy period and was not or was slightly reoriented by less than 20°N during storms (see Sect. 3.2.2.). We thus considered the storm surge direction as parallel to our transect.

The analyses of water level gradients, or slopes of the water surface, provide information on water level dynamics. Considering the short length of our instrumented transect (approximately 300 m), we calculated an instantaneous water level gradient between stations in cm.m^{-1}. A positive value indicates a positive slope of water surface (water level lower shore-ward than inland), and a negative value indicates a negative slope of water surface (water level higher shore-ward than inland). To analyze the water level gradient over the entire marsh platform, an additional calculation was made from WL2 to the most inland station (WL5) in cm.m^{-1}.

Several authors have evaluated the capacity of a coastal vegetated area to attenuate storm surge by a ratio of high water level (HWL) diminution per distance in cm or m per km along the entire marsh (Corps of Engineers, US Army Engineer District 1963; Krauss et al. 2009; Lovelace 1994; McGee et al. 2005; Wamsley et al. 2010; Zhang et al. 2012). HWL is the highest point reached by the water for a given period of time. We computed attenuation as a reduction of water level per distance of marsh between two stations at HWL for each tide cycle. For comparison with the literature, we also calculated an HWL attenuation rate over the marsh platform from WL2 to the most inland station (WL5) in cm.m^{-1}.

Results and Discussion

Environmental Context

During the fall of 2015, the marsh was characterized in terms of topography and vegetation biometry which are shown in Fig. 3.

Topography

The transect has elevations between −1.88 and 0.59 m and can be separated into three main parts: the submerged beach, the lower marsh, and the upper marsh (Fig. 3a). The submerged beach, 49.1 m long with a mean slope of 3.6 %, is delimited by the sharp marsh edge. The marsh platform edge forms a 0.7 m tall step from the submerged beach and marks the beginning of the lower marsh which extends to station 4 (WL4 and W4). This section has a length of 105 m and has an average slope of −0.01 %, representing a variation of 0 ± 0.25 m. However, this region of the marsh also contains the most important variation of topography and can further be separated in two main sections: the flat lower marsh (from stations 2 to 3) which is flat
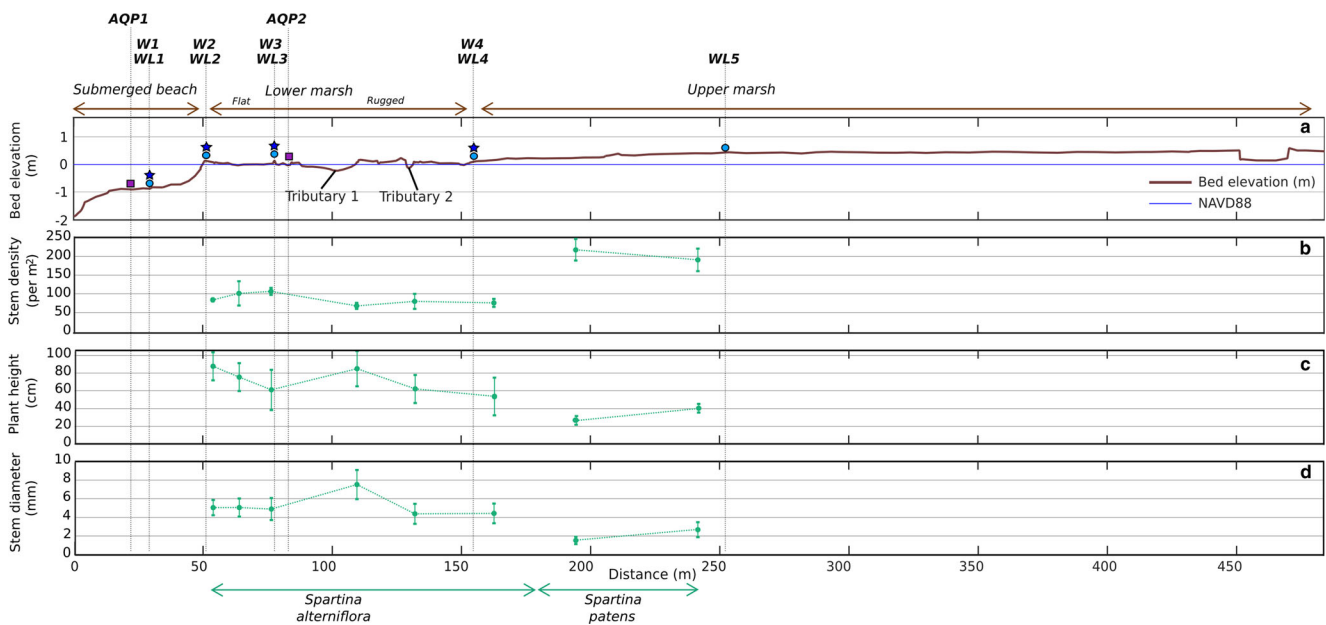
Fig. 3 Topography and vegetation characteristics measured along the transect. **a** Topography of the surveyed transect. Hydrodynamic measurement stations are represented by *purple squares* (AQP1 and AQP2), *light blue dots* (WL1 to WL5), and *dark blue stars* (W1 to W4). **b** Mean stem density per m^2. **c** Mean plant height in cm. **d** Mean stem diameter in mm. Plant species are noted at the bottom of the figure while marsh transect sections and hydrodynamic measurement stations are noted at the top

and does not present much variety of forms, and the rugged lower marsh (from stations 3 to 4) which is cut by two shallow streams (tributary 1 and 2) and presents a variety of bed forms. The upper marsh starts at station 4 and includes station 5. It is 350 m long presenting the highest elevations (0.15 to 0.59 m) and a slope of 0.11 %.

Vegetation Characteristics

The vegetation in the lower and upper marshes is dominated by *Spartina* species (Fig. 3b–d). The lower marsh (flat and rugged) is dominated by *Spartina alterniflora* while the upper marsh is dominated by *Spartina patens*. The *S. alterniflora* has higher mean stem densities (Fig. 3b) in the flat lower marsh (97 ± 20 stems.m^{-2}) than in the rugged lower marsh by about 30 stems per m^2. Mean plant heights of *S. alterniflora* (Fig. 3c) appeared to decrease overall along the lower marsh. However, these heights are considered constant (about 75 cm) along the lower marsh based on the wide variability observed. These values are two to three times higher than those made for the same species by Coulombier et al. (2012) in salt marshes in the St. Lawrence Estuary (Quebec, Canada). We attribute this to the warmer climate in Southern Virginia during the measurement period, mid-October 2015. Considering the variability of mean stem diameter in the lower marsh (Fig. 3d), we assumed a constant value (about 5 mm) except for an exceptionally high value landward of tributary 1 (7.52 ± 1.56 mm).

S. patens, dominating the upper marsh, has homogeneous mean stem densities of 217 ± 28 and 191 ± 30 stems.m^{-2} (Fig. 3b), considerably higher than the lower marsh vegetation

(by about 200 stems per m^2). Mean plant heights and stem diameters (Fig. 3c, d) increased between the two measurement stations (from 26.87 ± 4.81 cm to 40.53 ± 4.90 for mean height and from 1.53 ± 0.35 mm to 2.68 ± 0.80 for mean stem diameter) and are both lower than the assumed constant values for *S. alterniflora*. The vegetation of the upper marsh is thus denser than the vegetation of the lower marsh, but the plants are shorter and the diameter of the stems are thinner.

Hydrodynamics

Hydrodynamics were surveyed during two storm events. The first event lasted 5 days, from the 24th to the 29th of September 2015, and was characterized by strong winds from the North-Northeast (NNE) reaching 15.8 m s^{-1} at the storm peak (September 26th 2015, Fig. 4). The observed water levels recorded by NOAA's Tides and Currents Service at CBBT station (Fig. 1) during this storm show a particularly high tidal range of 1.3 m and a storm surge of 0.60 m above predicted astronomical tide levels (MSL + 0.6 m).

The second event, which also lasted 5 days, from the 1st to the 5th of October 2015, was a combination of an extra tropical storm, a particularly high astronomical tide and the influence of Hurricane Joaquin passing seaward of the U.S. East coast. During this event, the wind was blowing from the north (N) and reached 16.6 and 17.8 m.s^{-1} with two storm peaks, October 2nd and October 4th (Fig. 4). The NOAA observed tidal ranges at CBBT station for each storm peak were 1 and 0.7 m, respectively. The recorded storm surges at that station were particularly high, at 0.84 and 1 m, respectively, above
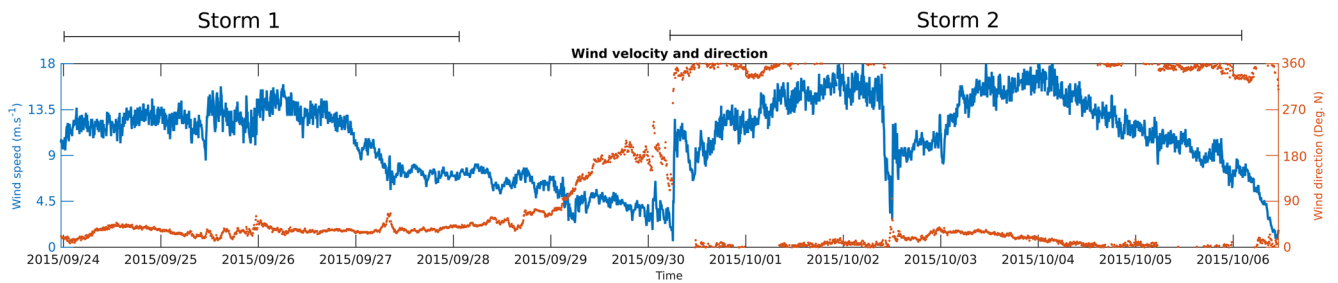
Fig. 4 Wind velocity (in m.s^{-1}) and wind direction (in °N) measured by NOAA at CBBT station during storm 1 and storm 2. Wind velocity is represented by the *blue line* while wind direction is represented by the *red dots*

predicted maximum tide levels (MSL + 0.63 m and MSL + 0.51 m, respectively).

Wave Characteristics

Waves were only observed for the first storm event, storm 1. During the peak storm tide cycle, H_s at W1 reached 0.34 m at high tide (Fig. 5a), then decreased at W2 (0.24 m), W3 (0.15 m), and W4 (0.07 m). At low tide, H_s values reached 0.07 m at W1 while no waves were recorded at other stations. The wave periods, T_p, (Fig. 5b) varied between 2.5 and 10 s at W1. The wave periods increased across the storm, particularly in the second part of the event after September 26th. At the beginning of the event, waves have short lengths and are thus wind waves generated locally. The increase of wave periods

across the storm indicates that a swell is propagated in the area from the ocean through the inlet fronting the Eastern Shore marsh. During the storm, periods are also increasing along the tide cycle. Due to the deeper water column, which allows the propagation of the swell over the marsh, wave periods increased over the rising tide and are the longest at high tide. Wave periods tend to be longer at ebb tide than at rising tide because of a slightly higher water level which allows the propagation of swell waves at the beginning of ebb tide.

The wave height decay rate (Fig. 5c) was most significant during the rising tide, followed by the ebb tide, and lowest at high tide. During the rising tide, the maximum decay rates were observed between W1 and W2 ($K_i = 0.045$ for the peak storm tide). Following the rising tide, the wave height decay is greatest between W2 and W3. Wave height decay was
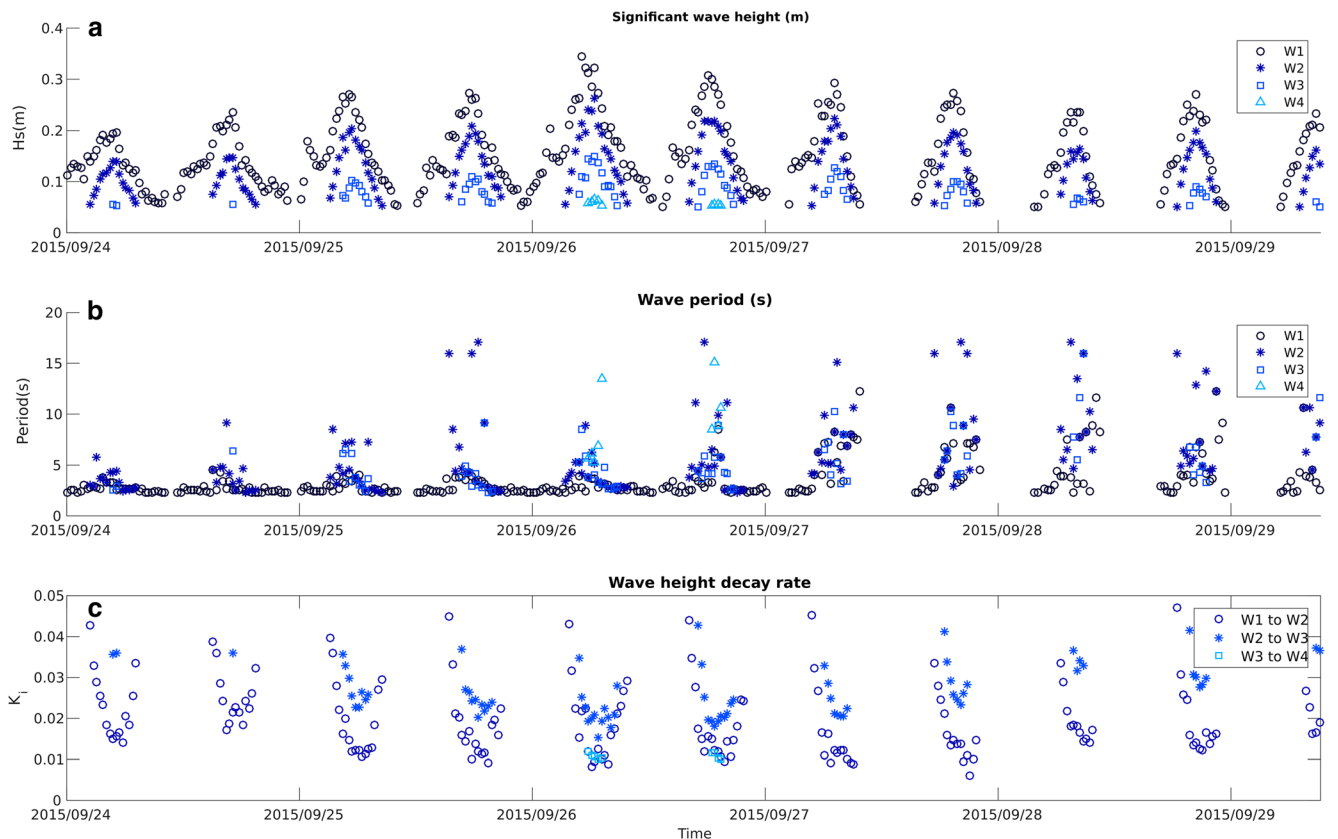

Fig. 5 Wave characteristics monitored during storm 1. **a** Significant wave height (in m). **b** Wave period (in s). **c** Wave height decay rate

observed between W3 and W4 during only two tide cycles corresponding to the storm peak. The rates between these two stations were equivalent to the decay rates observed between W1 and W2 during high tide, although the wave heights in these two sections were considerably different. We may thus conclude that most of the wave energy is attenuated in the flat lower marsh, between W2 and W3.

The increase of water level during the rising tide generates a transition of the greatest rates of attenuation from the marsh front edge (W1 to W2) to the flat lower marsh (W2 to W3). As the water depth increases, wave setup and wave breaking occur more inland. For the same reason, there is an attenuation of waves observed above the rugged lower marsh (W3 to W4) only during the high tides corresponding to the storm peak. As shown in Fig. 8a, there is a negative relationship between wave attenuation and water level; wave attenuation decreases when water level decreases. The greater wave attenuation during the rising tide in comparison to the ebb and high tide could be attributed to the increase of wave lengths along the tide cycle. It is expected that longer waves are less attenuated across the marsh. Bradley and Houser (2009) have shown that wave attenuation over seagrass is not uniform for all wave lengths as a function of the frequency of plant oscillation and lower frequency in the spectra tend to be more attenuated. No significant difference in vegetation effect on wave attenuation over the different sections studied was discernible since the vegetation had relatively similar stem diameters and plant heights.

Current Velocity and Direction

Current velocity and direction were monitored at stations AQP1 and AQP2 (Fig. 6). Mean velocity responded to the tidal cycle at both stations. At AQP1 (Fig. 6a), during the low energy period between storms, mean velocity over the entire water column was greatest during high tide (reaching 0.8 m.s^{-1}), was slower during rising and ebb tides (between 0.2 and 0.4 m.s^{-1}), and was slowest at low tide (less than 0.2 m.s^{-1}). During both events, the maximum mean velocity did not exceed 0.8 m.s^{-1}, but its vertical structure and evolution along the tidal cycle changed. At high tide, mean velocity was greatest in the top layer of the water column, hereafter referred to as the subsurface, and decreased around 0.4 m below the surface. These larger current velocities in the subsurface highlight the influence of wind shear stress at the water surface. The current velocities are vertically homogeneous under the subsurface due to the absence of vegetation in this area fronting the marsh.

In the low-energy period between storms, the mean current direction at AQP1 (Fig. 6b) is driven by the tide and is generally perpendicular to the WSW-ENE oriented shore (280°N). During both storms, the current direction in the subsurface was slightly redirected, about −20°N during storm 1 and −30°N

during storm 2, when compared to the low energy period between storms. Deeper in the water column, the redirection was less significant (respectively −20° and −10°N for storms 1 and 2). Closer to the bed, currents had the same direction as during low-energy periods. The reorientation of the mass of water is attributed to wind shear stress at the water surface. The moderate reorientation of the mass of water under the subsurface (less than 20°N) indicates that surge propagation dominates currents and is almost perpendicular to the shoreline.

Current mean velocity at AQP2, in the lower marsh, is slower than at AQP1 (maximum of 0.5 m.s^{-1} at the second storm peak, see Fig. 6c). During both events, higher current velocities in subsurface than on the rest of the water column were observed. Like at AQP1, we attribute this to wind shear stress at the water surface. In comparison to AQP1, the current velocities were strongly reduced in the entire water column which may be broadly attributed to the modification of the mass of water moving across the marsh by morphological features and the presence of vegetation. The morphological features along this transect which are expected to cause these changes include the marsh front edge, the presence of streams, and the presence of various small bed forms. We also expect the vegetation present to have had an impact on the reduction of mean velocities since *Spartina* species have been shown to decrease water velocities in the lower part of the water column (Leonard and Luther 1995; Neumeier 2007).

In the low energy period between storms, the mean current direction at AQP2 was primarily ESE directed with a few profiles heading WNW during the rising tide (Fig. 6d), indicating that there was a complete inundation of the marsh during rising tide followed by a complete draining for the rest of the cycle which corresponds to a straightforward bidirectional tidal movement in and out of the marsh.

During storm 1, we observed a similar cycle of filling and draining, but the upper part of the water column was reorientated by the dominant NNE winds (maximum +20°N). It is noteworthy that, during this storm, the lower part of the water column seems dominated by tides and not impacted by the surge as directions remained dominantly ESE, the direction of the tidal movement out of the marsh. This implies some impact of vegetation, particularly as this zone of low surge influence is about 0.6 m up the water column corresponding roughly to the mean vegetation height in this section of the transect.

During storm 2, the overall pattern observed during storm 1 remained, but the re-orientation of current impacted a thicker part of the water column and the changes in current direction through the water column were more progressive. The deeper re-orientation of current may be attributed to the re-orientation of water at the subsurface acting further downward due to a stronger wind during storm 2 while the mild progression of current direction through the water column could be due to the motion of vegetation under water acting to mix the current
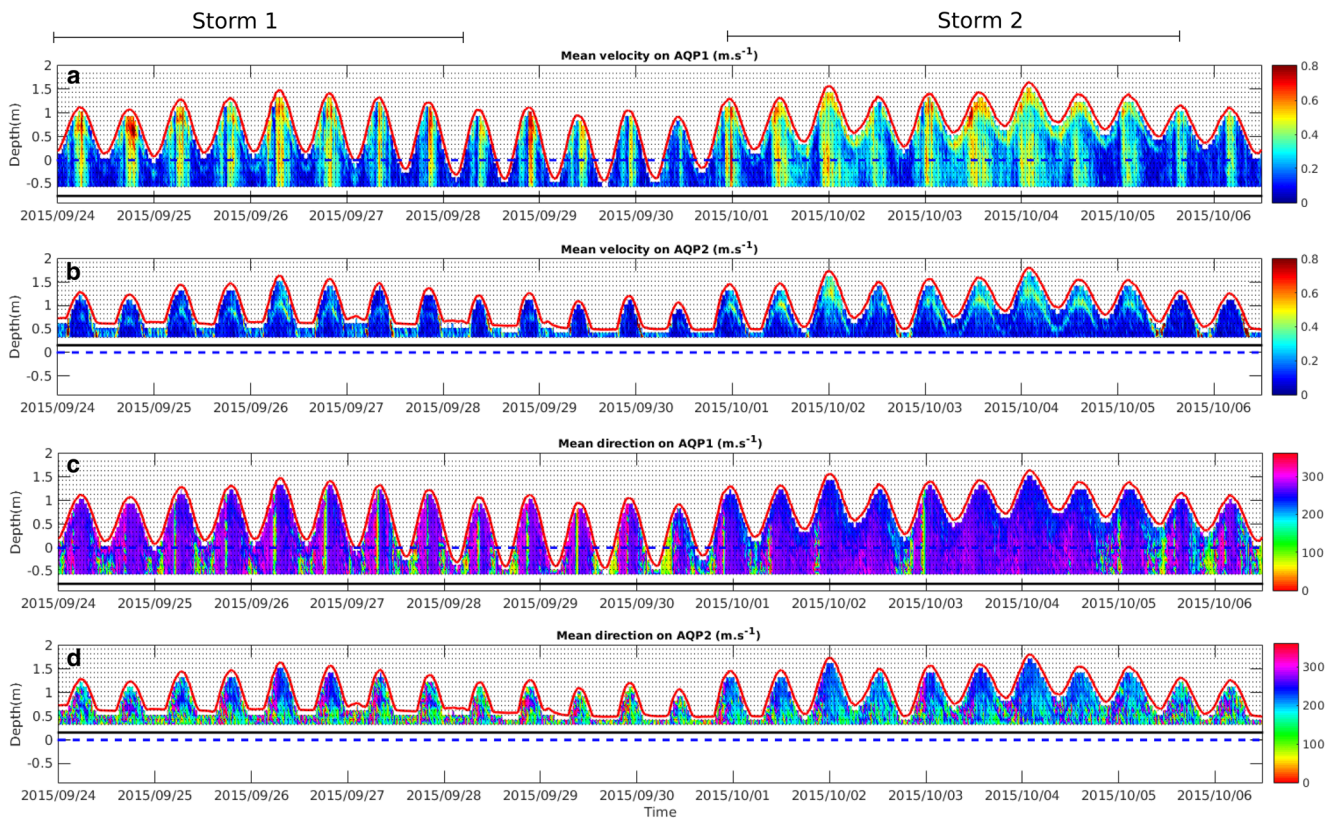
Fig. 6 Current mean velocity (in m.s^{-1}) at AQP1 (**a**) and AQP2 (**b**) and current mean direction (in °N) at AQP1 (**c**) and AQP2 (**d**). The *solid black lines* represent the bed elevation, the *blue dotted lines* represent the NAVD88 datum, and the *red lines* represent the water level measured by the ADCP pressure sensor. Cell heights are represented by the *black doted lines*

layers. With respect to the latter, several authors have observed plant bending due to currents in macro-algae and seagrass canopies (Boller and Carrington 2006; Fonseca et al. 1982; Paul et al. 2012). Videos made during field experiments (movie 1, accessible at https://vimeo.com/166043500) while the canopy was still half emergent (low tide at the beginning of storm 2) suggest that *Spartina* species can be bent by the currents in a similar fashion and can be subject to undulation under wave oscillation. The water level observed at AQP2 shows that the entire canopy was eventually submerged at high tide by at least twice the canopy height and can thus be considered as submerged vegetation. Ackerman and Okubo (1993) described an oscillatory movement of a seagrass canopy under unidirectional flow due to the hydro-elasticity of plants and named it "monami" which was supported by the results of others (Fonseca and Kenworthy 1987; Ghisalberti and Nepf 2002). As shown by Ghisalberti and Nepf (2009) and Nepf (2012), the combination of monami and deflection induces a greater flow speed within the canopy due to a better penetration of turbulent flux closer to the bed. Though we are not sure that monami can affect the more rigid *Spartina* canopies, we consider that the observed canopy bending and canopy undulation under current and wave effects (see movie 1) will allow a similar phenomenon and thus, also allow a penetration of the

re-oriented subsurface currents lower in the vertical profile. The fact that this process was not observed during storm 1 is explained by the results of Fonseca et al. (1982) which show that mean bending angle increases with current intensity. We expect that a threshold of current velocity was reached during storm 2 and not during storm 1.

In summary, the current velocity (i) is increased at the subsurface by wind shear stress at both stations and (ii) is strongly attenuated between AQP1 and AQP2 which seems linked to the roughness of the marsh (topography and vegetation). However, the interpretation of current direction is more challenging. Still, our observations allow us to develop potential hypotheses about the vertical distribution of the currents in the marsh area: (i) the wind shear stress at water surface seems to impact subsurface layer in terms of direction and speed and (ii) a layer influenced by the presence of vegetation occupies the lower part of the water column. The limit between these two layers becomes less defined as a function of the vegetation motion, itself controlled by current velocity and wave orbital velocity.

Water Level

Water levels measured at stations WL1 to WL5 are reported in Fig. 7a. As for wave heights and currents, water levels are
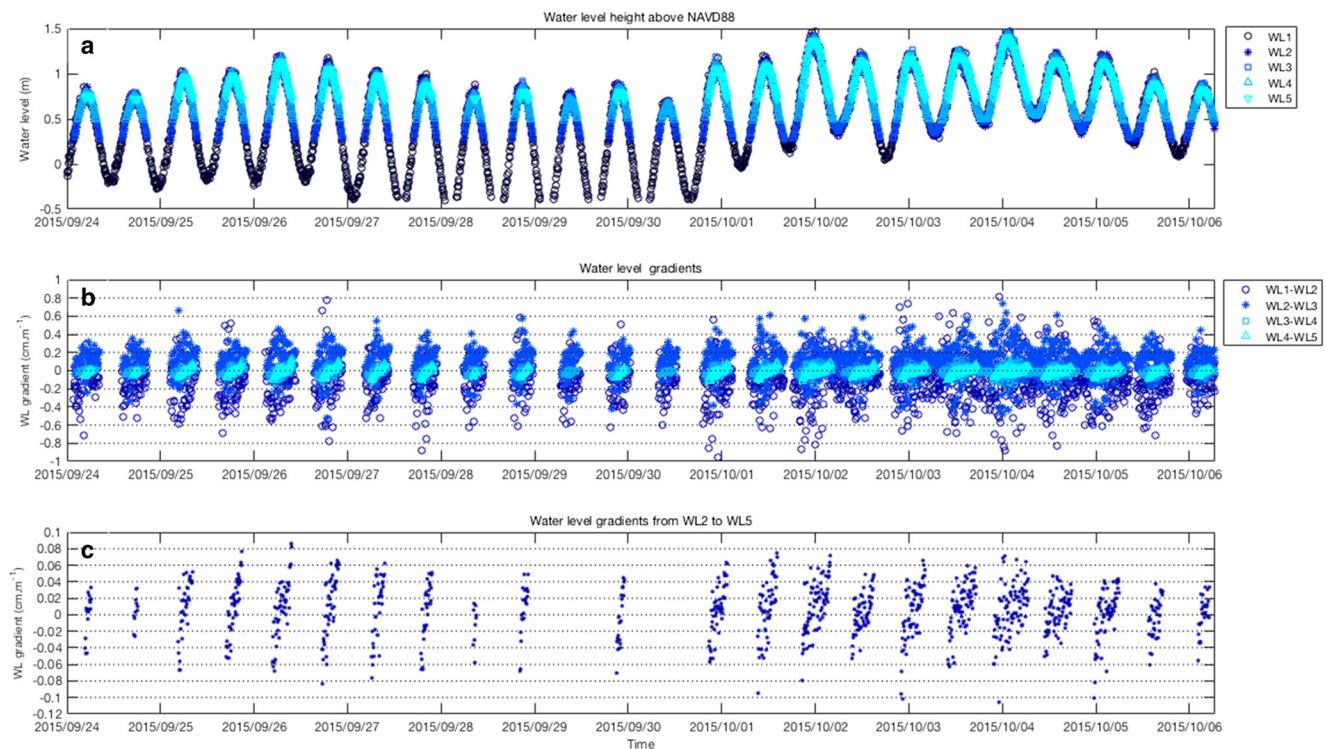
Fig. 7 **a** Water level at stations WL1 to WL5. **b** Water level gradients in cm.m^{-1} from station to station. **c** Water level gradients in cm.m^{-1} between stations WL2 and WL5 (over the entire marsh platform)

modulated by tides. As expected based on data from NOAA's CBBT station, during both storm events, the tidal range was reduced compared to the low energy period between the events.

The water level gradients in cm.m^{-1} were calculated from station to station (Fig. 7b) to analyze water surface slope over the different sections of the marsh and then, allowing for an understanding of water level dynamics. The majority of these values correspond to high tide periods since this computation requires recorded water levels at both stations. The water level gradient values are as follows: (i) mainly negative between WL1 and WL2 which translate to a negative slope of water surface above the front edge, (ii) mainly positive between WL2 and WL3 which translate to a positive slope of water surface above the flat lower marsh, and (iii) around zero between WL3 and WL4 and WL4 and WL5 which translate to small variations above the rugged low marsh and the upper marsh (from a negative slope of water surface at the beginning of the recorded tide cycle to a positive slope of water surface at the end of the cycle). Water level at WL1 is the highest, among other factors, because the wave heights (Fig. 5a) and wave setup are highest at the entrance of the marsh. As waves propagate across the marsh front edge, wave height (Fig. 5c) and wave setup (through wave breaking) should also decrease. Wave attenuation, by the reduction of wave height and wave setup, generates a reduction of instantaneous water level across the marsh front edge and explains the negative water

surface slope observed over this section. Along the flat lower marsh, the positive slope of water surface could be linked to a local augmentation of the water level at WL3. As waves are already attenuated over WL3 (except during the few tide cycles corresponding to the first storm peak as shown in Fig. 5c), wave setup is not a dominant process involved in this increase of water level. This phenomenon is more likely explained by the accumulation of water in the vicinity of WL3 due to surge propagating from the adjacent streams (ii). Over the rugged lower marsh and the upper marsh, gradients of water levels are small since wave dynamics are almost non-existent (Fig. 5) and current velocities reduced (Fig. 6) (iii). The decrease and inversion of water level gradients along the same tide cycle imply links to the progression of the tidal wave in and out the marsh.

Water level gradients in cm.m^{-1} have also been calculated from WL2 to WL5, over the marsh platform to exclude the effect of the marsh front edge (Fig. 7c). The water surface slope above the marsh is slightly negative at the end of rising tide, is flat at high tide, and is positive at the beginning of ebb tide which reflects the movement of the tidal wave across the marsh. The negative gradients (highest water level shoreward) have stronger absolute values than the positive gradients. As we observed a stronger wave attenuation during rising tide than ebb tide (Fig. 5c), we expect the variation of wave attenuation along the highest part of the tide cycle, even if smallest, to influence the water level gradients. The water

level gradients over such a small marsh are thus mainly linked to the movement of the tidal wave and to wave attenuation. In addition to waves and 3D circulation (here, progression of the tidal wave across the marsh and surge propagated by streams), wind could impact the water slope over the entire marsh platform by pushing the mass of water and then tend to give a negative slope to the water surface. However, we cannot demonstrate this effect in our results. The atmospheric pressure also certainly has a role in the augmentation of water level, but it will not influence the slope of the water surface since such a forcing will impact the entire marsh to the same extent.

Figure 8 shows scatter plots which illustrate the relationships between water level, water level gradient, wave attenuation, and wave height. Wave attenuation decreases when water level increases (Fig. 8a). A higher water column reduces the impact of the bed and submerged vegetation on wave modification and thus on wave attenuation. The augmentation of the submersion ratio (proportion of water column occupied

by vegetation) could also be part of this process as shown over seagrass meadows by others (Knutson et al. 1982; Koch 1999; Koch et al. 2009; Paul and Amos 2011; Ward et al. 1984).

Wave attenuation rates are highly dispersed for the lowest wave heights (0.05 to 0.2 m) and are low for wave heights of 0.2 to 0.4 m (Fig. 8b). Möller et al. (2014) established a positive relationship between wave height and wave attenuation for regular and irregular waves between 0.2 and 0.4 m. In our study, highest wave heights (over 0.3 m) are observed during high tide and correspond to the highest water level. Nevertheless, wave attenuation decreases when water level increases. Wave attenuation is thus lower for highest wave heights because of the high water levels correlated with them. The differences in wave attenuation values observed along the transect studied here may be a result of the non-linear interactions between water level, wave height, and the variety of bed forms of the natural marsh area.
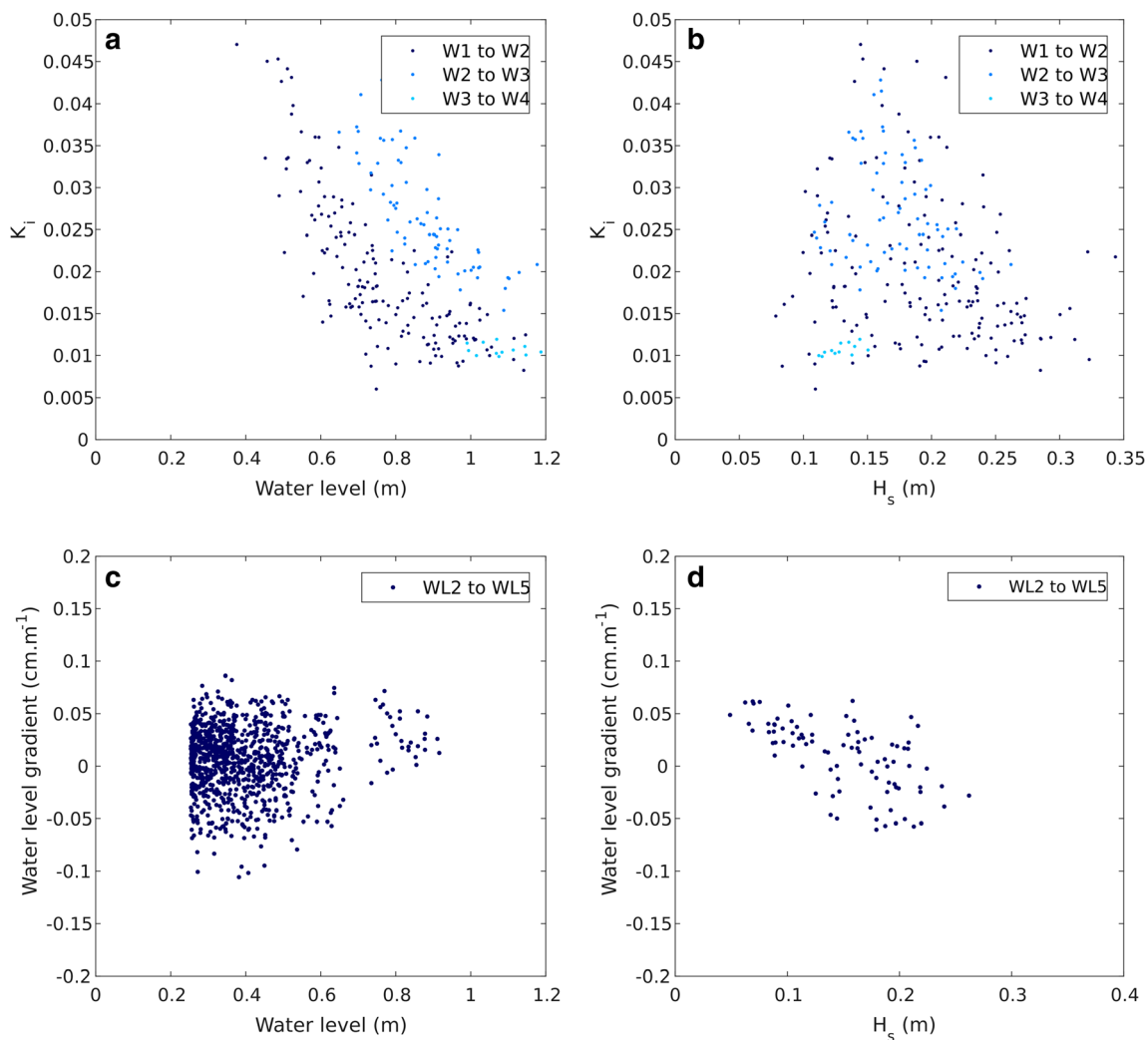

Fig. 8 Scatter plots showing relationships between wave attenuation rate and water level at WL1, WL2, and WL3 (a), wave attenuation rate and wave height at W1, W2, and W3 (b), water level gradients over the marsh platform and water level at WL2 (c) water level gradients over the marsh platform and wave height at W2 (d)

No relationship was discernible in our dataset between water level gradients and a water level lower than NAVD88 + 0.7 m (Fig. 8c). For a higher water column, water level gradients were mainly positive. This suggests that for high water levels, the water surface shows a positive slope possibly due to an increase of the water level along the marsh, likely linked to a movement of wave setup inland helped by the higher water level as observed by Jago et al. (2007) over a coral reef flat in Australia.

Our dataset also shows that water level gradients are negatively correlated with wave height at the entrance of the marsh (Fig. 8d). As expected, the wave dynamics have a strong influence on water level height around the marsh front edge since water level is higher shore-ward of the meadow front edge due to the influence of wave setup and wave height and decreases across the marsh thanks to, among other factors, wave attenuation processes.

HWL attenuation rates have been calculated over the same sections (from station to station and over the marsh) for 24 high tide peaks (22 from WL4 to WL5). The HWL attenuation values in function of incoming HWL and HWL

attenuation over the entire marsh in function of wave attenuation across the marsh front edge are presented in Fig. 9a–d. From station to station, the HWL attenuation rates are mainly positive (until 0.26 cm.m^{-1} from WL1 to WL2, 0.23 from WL2 to WL3, 0.13 from WL3 to WL4, and 0.06 from WL4 to WL5). The marsh front edge (from WL1 to WL2) and the flat lower marsh (WL2 to WL3) exhibit the highest attenuation rates but also negative rates (decreasing respectively until −0.1 and −0.18 cm.m^{-1}). The different sections of the marsh are efficient in reducing storm surge. The shore-ward sections (marsh front edge and flat lower marsh) have the most variability in HWL attenuation values, attributable to the higher variation of water level generated by waves which are not yet attenuated in the shoreline area (Fig. 5c). The rugged lower marsh and especially the upper marsh are less efficient in storm surge attenuation. The rugged lower marsh is slightly more efficient at reducing water level than the upper marsh, though the latter has a higher bed slope. This could be linked to the more significant roughness of the rugged lower marsh due to either the variations in topography, the characteristics of
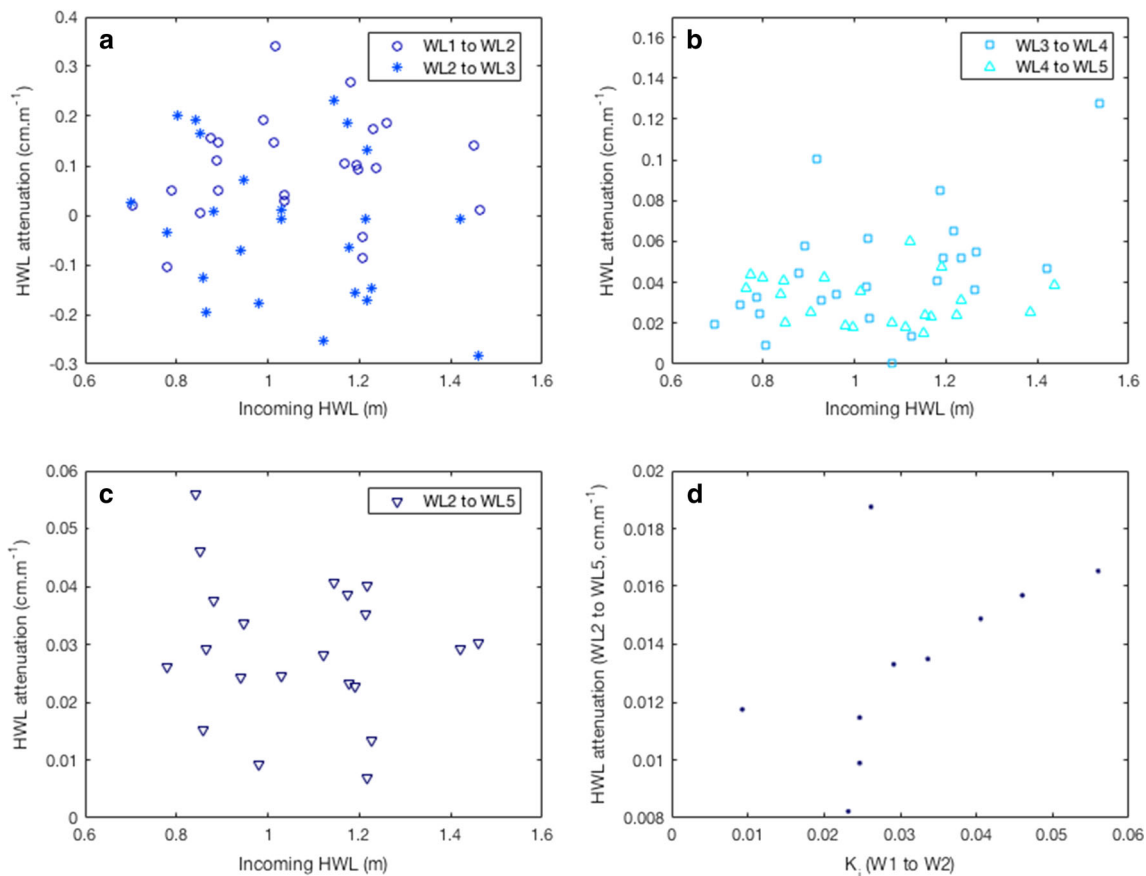

Fig. 9 Scatter plots of high water level (HWL) attenuation rates in cm.m^{-1} from station to station in function of the incoming HWL, from stations WL1 to WL2 (over the marsh edge) and WL2 to WL3 (over the flat lower marsh) (a), from stations WL3 to WL4 (rugged lower marsh) and WL4 to WL5 (upper marsh) (b), and from station WL2 to WL5 (over the entire marsh platform) (c). Scatter plot of relationship between wave decay rate over the marsh front edge (W2 to W3) at the time of HWL against HWL attenuation rate over the marsh platform (d)

vegetation (denser but lower and more flexible considering smaller stem diameters in the upper marsh), or a combination of both.

HWL attenuation over the entire platform is always positive; the marsh platform always attenuates storm surge in the limit of the surges we observed. The analysis of the data did not demonstrate a relationship between HWL attenuation and the incoming HWL or the incoming water level relative to the marsh platform, like observed by Stark et al. (2015). We did not find any relationship with wave height at the entrance of the marsh. However, we cannot also certify that no relationship exists, since the number of values observed is significantly small compared to our analysis of water level gradients. Moreover, while it is not easy to relate HWL attenuation to wave height or water level, Fig. 9d shows a positive relationship between HWL attenuation over the entire marsh platform and the wave attenuation observed across the marsh

Table 1 Water level attenuation rates observed by other authors in the field or by modeling, based and expanding on the literature review conducted by Stark et al. (2015)

Authors	Data source	Surge type	Wetland type	Location	Length of attenuation (km)	Attenuation rate (cm.km^{-1})
1. Lovelace 1994 in Wamsley et al. 2010	Field	Hurricane Andrew, 1992	Marsh/open water	Louisiana, USA	37	4.4 to 4.9
2. In Stark et al. 2015, calculated from figures in Van der Molen, 1997	Field	Tides	Tidal flat/marsh channel	Massachusetts, USA	-	−2.0 to 11.0
3. Krauss et al. 2009	Field	Hurricane Charley, 2004	Marsh/mangrove	Florida, USA	5.5	9.4 to 15.8
4. Krauss et al. 2009	Field	Hurricane Wilma, 2005	Marsh/mangrove	Florida, USA	14	4.0 to 6.9
5. McGee et al. 2006, Wamsley et al. 2010	Field	Hurricane Rita, 2005	Marsh	Louisiana, USA	-	10.0
6. Mc Gee et al. 2006, Wamsley et al. 2010	Field	Hurricane Rita, 2005	Marsh	Louisiana, USA	-	25.0
7. McGee et al. 2006, Wamsley et al. 2010	Field	Hurricane Rita, 2005	Marsh	Louisiana, USA	-	4.0
8. Mc Gee et al. 2006, Wamsley et al. 2010	Field	Hurricane Rita, 2005	Marsh	Louisiana, USA	-	7.7
9. Zhang et al. 2012	Modeling	Hurricane Wilma, 2005	Mangrove	Louisiana, USA	6–30	40 to 50
10. Zhang et al. 2012	Modeling	Hurricane Wilma, 2005	Mangrove/open water	Louisiana, USA	6–30	20
11. Stark et al. 2015, evaluated from figures	Field	Tides and storm surge	Marsh platform, edge of a small stream	Netherlands	~0.15	−2 to 70
12. Stark et al. 2015, evaluated from figures	Field	Tides and storm surge	Marsh platform, edge of a small stream	Netherlands	~0.1	−2 to 60
13. Stark et al. 2015, evaluated from figures	Field	Tides and storm surge	Marsh platform, edge of the main stream (~100 m wide)	Netherlands	~0.05	25 to 65
14. Present study	Field	Tides and storm surge	Marsh platform	Virginia, USA	0.25	15 to 60
15. Present study	Field	Tides and storm surge	Marsh front edge	Virginia, USA	0.02	−100 to 270
16. Present study	Field	Tides and storm surge	Flat lower marsh	Virginia, USA	0.02	−280 to 230
17. Present study	Field	Tides and storm surge	Rugged lower marsh (channels)	Virginia, USA	0.07	0 to 120
Present study	Field	Tides and storm surge	Upper marsh	Virginia, USA	0.09	15 to 60

front edge. This trend reflects that wave attenuation across the marsh front edge, by decreasing wave height (Fig. 5) and subsequently reducing wave setup, induces a decreasing of water level contributing to the attenuation of HWL over the entire marsh.

The storm surge (or HWL) attenuation rates observed over the marsh platform are higher than those observed in the field or modeled by other authors in marshes under hurricane impact (Table 1, lines 1 to 8). They are of the same order as the values obtained through modeling by Zhang et al. (2012) reported here in Table 1, lines 9 and 10 in a mangrove under hurricane Wilma's impact. We can expect that hurricanes generate higher surge than a seasonal storm but a mangrove has higher capacity to attenuate a storm surge than a marsh.

The work of Stark et al. (2015), reported here in Table 1, lines 11 to 13, in an estuarine tidal marsh on the North Sea (Netherlands), allows the comparison of HWL attenuation over short marsh sections. The sections for which Stark et al. present HWL attenuation values are cut by streams and include marsh edges. In our study, we observed higher values than Stark et al. in the near-shore area, which also present a marsh edge. The propagation of waves is potentially less important in this estuary than at our field site which is relatively exposed to the Atlantic Ocean. Our study has shown that wave height reduction (Fig. 5) and thereby wave setup reduction, occurring during wave attenuation across the marsh front edge, are an important process in HWL attenuation. Therefore, the more significant wave propagation on our site could explain the higher positive attenuation rates in the near-shore area as compared to Stark et al. (2015). This higher positive attenuation is associated to wave conditions in a more energetic environment since wave setup is here increasing the water level shore-ward. The HWL attenuation values observed by Stark et al. (2015) are slightly lower than what we observed in the rugged lower marsh (also cut by streams) and close to what was observed in the upper marsh. Stark et al. (2015) does not provide a detailed description of the vegetation over the studied transect, but the mean canopy height of their most abundant species is about 0.43 ± 0.1 m. This is lower than the height of *Spartina alterniflora* observed in the rugged lower marsh (0.67 ± 0.2 m). The lower canopy height could explain why they observed lower attenuation values. The canopy height of their most abundant species is slightly higher than the height of *Spartina patens* observed in the upper marsh and where we observed attenuation rates similar to theirs. However, there is no major stream in the upper marsh. Marsh continuity could thus play a role in these variations of storm surge attenuation, which lends field-data driven support to the numerical modeling work done by Loder et al. (2009) for an idealized marsh area, which included sensitivity studies of marsh continuity.

Conclusions and Further Studies

The main goals of the present study have been to quantify storm surge attenuation over a marsh area while improving the understanding of the variability and interactions of the processes involved and their contribution to storm surge attenuation. To that aim, we have collected a high-resolution dataset in a natural environment over a cross-shore transect in a coastal wetland at the mouth of the Chesapeake Bay during two storm events in the Fall of 2015. The collected data included marsh morphology, vegetation characteristics across the transect, wave characteristics, and current velocity and direction evolution along the marsh transect. These were examined with the aim of understanding the evolution of storm surge (water level) and its propagation along the marsh. The main findings of this analysis can be summarized as follows:

1. This marsh area, despite its short length, attenuates waves, reduces current velocity, and attenuates high water level.
2. Current velocities and directions in front of the marsh and at the marsh platform are driven by tides, while current velocities beyond the marsh platform are strongly reduced compared to the current in front of the marsh.
3. Wave attenuation varies with water level along the tide cycle. The increase in water level decreases the modification of the waves by the marsh. Wave attenuation is thus less important at high tide than at low tide.
4. On one hand, the negative slope of water surface (highest water level shore-ward) over such a short length of marsh is linked to wave setup at the entrance of the marsh and, thus, to wave attenuation across the marsh. As wave height and wave setup are larger shore-ward than inland, the instantaneous water level is higher shore-ward than inland which explains the negative slope of water surface. On the other hand, the wave attenuation across the marsh is limited when the water level increases and can thus limit the negative slope of water surface. The water level gradients over such a small marsh are also linked to the movement of the tidal wave in and out the marsh.
5. High water level attenuation is linked to wave attenuation which, by decreasing wave setup across the marsh front edge, induces a reduction of water level contributing to the attenuation of high water level over the entire marsh.
6. The high water level attenuation rates observed here have a greater range than the rates observed or modeled by other authors and this may be linked to the strong influence of waves in storm surge attenuation over coastal areas.

In the present study, the major challenge has been in linking the attenuation of the different storm surge components, including water level gradients, and attenuation

with the vegetation and the morphology characteristics along the marsh. Several studies have been conducted by other authors to evaluate submerged or emerged vegetation biometry influence on waves (e.g., Tschirky et al. 2001), currents (e.g., Wu et al. 1999), and wave-current interactions (Lara et al. 2016; Maza et al. 2015). To our knowledge, the influence of marsh morphology and vegetation biometry on water level attenuation in realistic conditions has been rarely explored and could give key answers in the use of natural defenses in coastal management. These questions could be addressed by future laboratory and modeling studies including simulations of realistic hydrodynamic conditions over non-vegetated beds and vegetated beds presenting different biometric characteristics to further explore the contribution of each component in water level attenuation. Modeling studies could also be used to evaluate if, aside from the influence of the criteria discussed in this study, particularly waves, the length of the marsh would influence water level attenuation and, if yes, what processes are involved. While this topic has been assessed by Stark et al. (2016) in a recent publication about a modeling study, there remains a need for better parameterization of vegetation resistance in such models, particularly in coastal settings. Field studies and lab studies which aim to quantify the relative contributions of vegetative and bed-form drag can contribute to reach a better parametrization. We hope that the observations of the present study can provide insights into setting up and executing future field and lab studies for this purpose, a particular challenge in storm conditions. In the present study, we hypothesize that, under strong hydrodynamic conditions, the interactions between wind shear stress penetration in the water column and vegetation motion under hydrodynamic influence result in a modification of the current vertical repartition. To our knowledge, these questions have also not been explored in coastal marsh areas.

References

Ackerman, J.D., and A. Okubo. 1993. Reduced mixing in a marine Macrophyte canopy. *Functional Ecology* 7: 305–309. doi:10.2307/2390209.

Anderson, M.E., and J.M. Smith. 2014. Wave attenuation by flexible, idealized salt marsh vegetation. *Coastal Engineering* 83: 82–92. doi:10.1016/j.coastaleng.2013.10.004.

Arkema, K.K., G. Guannel, G. Verutes, S.A. Wood, A. Guerry, M. Ruckelshaus, P. Kareiva, M. Lacayo, and J.M. Silver. 2013. Coastal habitats shield people and property from sea-level rise and storms. *Nature Climate Change* 3: 913–918. doi:10.1038/nclimate1944.

Boller, M.L., and E. Carrington. 2006. In situ measurements of hydrodynamic forces imposed on *Chondrus crispus* Stackhouse. *Journal of Experimental Marine Biology and Ecology* 337: 159–170. doi:10.1016/j.jembe.2006.06.011.

Bouma, T.J., M.B. De Vries, E. Low, G. Peralta, I.C. Tanczos, J. Van de Koppel, and P.M.J. Herman. 2005. Trade-offs related to ecosystem engineering: a case study on stiffness of emerging macrophytes. *Ecology* 86: 2187–2199.

Bouma, T.J., J. van Belzen, T. Balke, Z. Zhu, L. Airoldi, A.J. Blight, A.J. Davies, C. Galvan, S.J. Hawkins, S.P.G. Hoggart, J.L. Lara, I.J. Losada, M. Maza, B. Ondiviela, M.W. Skov, E.M. Strain, R.C. Thompson, S. Yang, B. Zanuttigh, L. Zhang, and P.M.J. Herman. 2014. Identifying knowledge gaps hampering application of intertidal habitats in coastal protection: opportunities & steps to take. *Coastal Engineering* 87: 147–157. doi:10.1016/j.coastaleng.2013.11.014.Coasts@Risks: THESEUS, a new wave in coastal protection

Bradley, K., Houser, C. 2009. Relative velocity of seagrass blades : Implications for wave attenuation in low-energy environments. *Journal of Geophysical Research - Earth Surface* 114. doi:10.1029/2007JF000951.

Bridges, T.S., Wagner, P.W., Burks-Copes, K.A., Bates, M., Collier, Z.A. 2015. Use of natural and nature-based features (NNBF) for coastal resilience (Final Report No. ERDC SR-15-1). USACE-ERDC

Committee on Environment, Natural, Resources, and Sustainability, National Science and Technology Council. 2015. *Ecosystem-service assessment: research needs for coastal green infrastructure.* Executive Office of the President of the United States

Corps of Engineers, US Army Engineer District. 1963. *Interim survey report: Morgan City, Louisiana and vicinity (No. Serial no. 63).* New Orleans, Louisiana

Coulombier, T., U. Neumeier, and P. Bernatchez. 2012. Sediment transport in a cold climate salt marsh (St. Lawrence estuary, Canada), the importance of vegetation and waves. *Estuarine, Coastal and Shelf Science* 101: 64–75. doi:10.1016/j.ecss.2012.02.014.

Fonseca, M.S., and W.J. Kenworthy. 1987. Environmental impacts on seagrasses effects of current on photosynthesis and distribution of seagrasses. *Aquatic Botany* 27: 59–78. doi:10.1016/0304-3770(87)90086-6.

Fonseca, M.S., J.S. Fisher, J.C. Zieman, and G.W. Thayer. 1982. Influence of the seagrass, *Zostera marina* L., on current flow. *Estuarine, Coastal and Shelf Science* 15: 351–364. doi:10.1016/0272-7714(82)90046-4.

Gedan, K.B., M.L. Kirwan, E. Wolanski, E.B. Barbier, and B.R. Silliman. 2011. The present and future role of coastal wetland vegetation in protecting shorelines: answering recent challenges to the paradigm. *Climatic Change* 106: 7–29. doi:10.1007/s10584-010-0003-7.

Ghisalberti, M., and H.M. Nepf. 2002. Mixing layers and coherent structures in vegetated aquatic flows. *Journal of Geophysical Research, Oceans* 107: 3–1. doi:10.1029/2001JC000871.

Ghisalberti, M., and H. Nepf. 2009. Shallow flows over a permeable medium: the hydrodynamics of submerged aquatic canopies. *Transport in Porous Media* 78: 309–326. doi:10.1007/s11242-008-9305-x.

Horikawa, K. 1988. *Nearshore dynamics and coastal processes : theory, measurement and predictive models*, 1–522. Tokyo: University of Tokyo Press.

Hu, K., Q. Chen, and H. Wang. 2015. A numerical study of vegetation impact on reducing storm surge by wetlands in a semi-enclosed estuary. *Coastal Engineering* 95: 66–76. doi:10.1016/j.coastaleng.2014.09.008.

Jadhav, R., and Q. Chen. 2012. Field investigation of wave dissipation over salt marsh vegetation during tropical cyclone. *Coastal Engineering Proceedings* 1(33): 41. doi:10.9753/icce.v33.waves.41.

Jago, O.K., Kench, P.S., Brander, W.S. 2007. Field observations of wave-driven water-level gradients across a coral reef flat. *Journal of Geophysical Research - Oceans* 112. doi:10.1029/2006JC003740.

John, B.M., K.G. Shirlal, and S. Rao. 2015. Effect of artificial vegetation on wave attenuation – an experimental investigation. *Procedia Eng.* 116: 600–606. doi:10.1016/j.proeng.2015.08.331.

Knutson, P.L., R.A. Brochu, W.N. Seelig, and M. Inskeep. 1982. Wave damping In*spartina alterniflora* marshes. *Wetlands* 2: 87–104. doi:10.1007/BF03160548.

Koch, E.W. 1999. Sediment resuspension in a shallow *Thalassia testudinum* banks ex König bed. *Aquatic Botany* 65: 269–280.

Koch, E.W., E.B. Barbier, B.R. Silliman, D.J. Reed, G.M. Perillo, S.D. Hacker, E.F. Granek, J.H. Primavera, N. Muthiga, S. Polasky, B.S. Halpern, C.J. Kennedy, C.V. Kappel, and E. Wolanski. 2009. Non-linearity in ecosystem services: temporal and spatial variability in coastal protection. *Frontiers in Ecology and the Environment* 7: 29–37. doi:10.1890/080126.

Krauss, K.W., T.W. Doyle, T.J. Doyle, C.M. Swarzenski, A.S. From, R.H. Day, and W.H. Conner. 2009. Water level observations in mangrove swamps during two hurricanes in Florida. *Wetlands* 29: 142–149. doi:10.1672/07-232.1.

Lara, J.L., M. Maza, B. Ondiviela, J. Trinogga, I.J. Losada, T.J. Bouma, and N. Gordejuela. 2016. Large-scale 3-D experiments of wave and current interaction with real vegetation. Part 1: guidelines for physical modeling. *Coastal Engineering* 107: 70–83. doi:10.1016/j.coastaleng.2015.09.012.

Lavoie, R., J. Deslandes, and F. Proulx. 2016. Assessing the ecological value of wetlands using the MACBETH approach in Quebec City. *Journal for Nature Conservation* 30: 67–75. doi:10.1016/j.jnc.2016.01.007.

Leonard, L.A., and A.L. Croft. 2006. The effect of standing biomass on flow velocity and turbulence in *Spartina alterniflora* canopies. *Estuarine, Coastal and Shelf Science* 69: 325–336. doi:10.1016/j.ecss.2006.05.004.Salt Marsh Geomorphology: Physical and ecological effects on landform

Leonard, L.A., and M.E. Luther. 1995. Flow hydrodynamics in tidal marsh canopies. *Limnology and Oceanography* 40: 1474–1484. doi:10.4319/lo.1995.40.8.1474.

Leonard, L.A., A.C. Hine, and M.E. Luther. 1995. Surficial sediment transport and deposition processes in a *Juncus roemerianus* marsh, west-Central Florida. *Journal of Coastal Research* 11: 322–336.

Loder, N.M., J.L. Irish, M.A. Cialone, and T.V. Wamsley. 2009. Sensitivity of hurricane surge to morphological parameters of coastal wetlands. *Estuarine, Coastal and Shelf Science* 84: 625–636. doi:10.1016/j.ecss.2009.07.036.

Lott, N., Ross, T. 2006. *1.2 Tracking and evaluating US billion dollar weather disasters, 1980–2005*. Retrieved on March

Lovelace, J.K., 1994. *Storm-tide elevations produced by hurricane Andrew along the Louisiana Coast, August 25–27, 1992 (No. 94–371)*. U.S. Geological Survey

Marsooli, R., and W. Wu. 2014. Numerical investigation of wave attenuation by vegetation using a 3D RANS model. *Advances in Water Resources* 74: 245–257. doi:10.1016/j.advwatres.2014.09.012.

Maza, M., J.L. Lara, I.J. Losada, B. Ondiviela, J. Trinogga, and T.J. Bouma. 2015. Large-scale 3-D experiments of wave and current interaction with real vegetation. Part 2: experimental analysis. *Coastal Engineering* 106: 73–86. doi:10.1016/j.coastaleng.2015.09.010.

McGee, B.D., Tollett, R.W., Goree, B.B., Farris, G.S., Smith, G.J., Crane, M.P., Demas, C.R., Robbins, L.L., Lavoie, D.L. 2005. Monitoring Hurricane Rita inland storm surge. *Science and the Storms: the USGS Response to the Hurricane* 257–263

McGee, B.D., Goree, B.B., Tollett, R.W., Woodward, B.K., Kress, W.H., 2006. Hurricane Rita surge data, Southwestern Louisiana and Southeastern Texas, September to November 2005. US Geological Survey Data Series 220. https://pubs.usgs.gov/ds/2006/220/.

Möller, I., T. Spencer, J.R. French, D. Leggett, and M. Dixon. 1999. Wave transformation over salt marshes: a field and numerical modelling study from North Norfolk, England. *Estuarine, Coastal and Shelf Science* 49: 411–426.

Möller, I., M. Kudella, F. Rupprecht, T. Spencer, M. Paul, B.K. van Wesenbeeck, G. Wolters, K. Jensen, T.J. Bouma, M. Miranda-Lange, and S. Schimmels. 2014. Wave attenuation over coastal salt marshes under storm surge conditions. *Nature Geoscience* 7: 727–731. doi:10.1038/ngeo2251.

Nepf, H.M. 1999. Drag, turbulence, and diffusion in flow through emergent vegetation. *Water Resources Research* 35: 479–489.

Nepf, H.M. 2012. Flow and transport in regions with aquatic vegetation. *Annual Review of Fluid Mechanics* 44: 123–142. doi:10.1146/annurev-fluid-120710-101048.

Neumeier, U. 2007. Velocity and turbulence variations at the edge of saltmarshes. *Continental Shelf Research* 27: 1046–1059. doi:10.1016/j.csr.2005.07.009.

Neumeier, U., Ciavola, P. 2004. Flow resistance and associated sedimentary processes in a *Spartina maritima* Salt-Marsh. *Journal of Coastal Research* 435–447. doi:10.2112/1551-5036(2004)020[0435:FRAASP]2.0.CO;2

Paul, M., and C.L. Amos. 2011. Spatial and seasonal variation in wave attenuation over *Zostera noltii*. *J. Geophys. Res.-Oceans* 116: C08019. doi:10.1029/2010JC006797.

Paul, M., T. Bouma, and C. Amos. 2012. Wave attenuation by submerged vegetation: combining the effect of organism traits and tidal current. *Marine Ecology Progress Series* 444: 31–41. doi:10.3354/meps09489.

Peralta, G., L. van Duren, E. Morris, and T. Bouma. 2008. Consequences of shoot density and stiffness for ecosystem engineering by benthic macrophytes in flow dominated areas: a hydrodynamic flume study. *Marine Ecology Progress Series* 368: 103–115. doi:10.3354/meps07574.

Perry, J.E., Barnard, T.A., Bradshaw, J.G., Friedrichs, C.T., Havens, K.J., Mason, P.A., Priest, W.I., Silberhorn, G.M. 2001. Creating Tidal Salt Marshes in the Chesapeake Bay. *Journal of Coastal Research* 170–191

Resio, D.T., and J.J. Westerink. 2008. Modeling the physics of storm surges. *Physics Today* 61: 33–38. doi:10.1063/1.2982120.

Sénéchal, N., H. Dupuis, P. Bonneton, H. Howa, and R. Pedreros. 2001. Observation of irregular wave transformation in the surf zone over a gently sloping sandy beach on the French Atlantic coastline. *Oceanologica Acta* 24: 545–556.

Sheng, Y.P., A. Lapetina, and G. Ma. 2012. The reduction of storm surge by vegetation canopies: three-dimensional simulations. *Geophysical Research Letters* 39: L20601. doi:10.1029/2012GL053577.

Shepard, C.C., C.M. Crain, and M.W. Beck. 2011. The protective role of coastal marshes: a systematic review and meta-analysis. *PloS One* 6: e27374. doi:10.1371/journal.pone.0027374.

Spalding, M.D., A.L. McIvor, M.W. Beck, E.W. Koch, I. Möller, D.J. Reed, P. Rubinoff, T. Spencer, T.J. Tolhurst, T.V. Wamsley, B.K. van

Wesenbeeck, E. Wolanski, and C.D. Woodroffe. 2014a. Coastal ecosystems: a critical element of risk reduction. *Conservation Letters* 7: 293–301. doi:10.1111/conl.12074.

Spalding, M.D., S. Ruffo, C. Lacambra, I. Meliane, L.Z. Hale, C.C. Shepard, and M.W. Beck. 2014b. The role of ecosystems in coastal protection: adapting to climate change and coastal hazards. *Ocean and Coastal Management* 90: 50–57. doi:10.1016/j.ocecoaman.2013.09.007.

Stark, J., T. Van Oyen, P. Meire, and S. Temmerman. 2015. Observations of tidal and storm surge attenuation in a large tidal marsh. *Limnology and Oceanography* 60: 1371–1381. doi:10.1002/lno.10104.

Stark, J., Y. Plancke, S. Ides, P. Meire, and S. Temmerman. 2016. Coastal flood protection by a combined nature-based and engineering approach: modeling the effects of marsh geometry and surrounding dikes. *Estuarine, Coastal and Shelf Science* 175: 34–35. doi:10.1016/j.ecss.2016.03.027.

Sutton-Grier, A.E., K. Wowk, and H. Bamford. 2015. Future of our coasts: the potential for natural and hybrid infrastructure to enhance the resilience of our coastal communities, economies and ecosystems. *Environmental Science & Policy* 51: 137–148. doi:10.1016/j.envsci.2015.04.006.

Thomas, R.E., M.F. Johnson, L.E. Frostick, D.R. Parsons, T.J. Bouma, J.T. Dijkstra, O. Eiff, S. Gobert, P.-Y. Henry, P. Kemp, S.J. Mclelland, F.Y. Moulin, D. Myrhaug, A. Neyts, M. Paul, W.E. Penning, S. Puijalon, S.P. Rice, A. Stanica, D. Tagliapietra, M. Tal, A. Tørum, and M.I. Vousdoukas. 2014. Physical modelling of water, fauna and flora: knowledge gaps, avenues for future research

and infrastructural needs. *Journal of Hydraulic Research* 52: 311–325. doi:10.1080/00221686.2013.876453.

Tschirky, P., Hall, K., Turcke, D. 2001. Wave attenuation by emergent wetland vegetation. In: *Coastal engineering conference*. ASCE American Society Of Civil Engineers, pp. 865–877

Wamsley, T.V., M.A. Cialone, J.M. Smith, J.H. Atkinson, and J.D. Rosati. 2010. The potential of wetlands in reducing storm surge. *Ocean Engineering* 37: 59–68. doi:10.1016/j.oceaneng.2009.07.018.A Forensic Analysis of Hurricane Katrina's Impact: Methods and Findings

Ward, L.G., W. Michael Kemp, and W.R. Boynton. 1984. The influence of waves and seagrass communities on suspended particulates in an estuarine embayment. *Marine Geology* 59: 85–103. doi:10.1016/0025-3227(84)90089-6.

Wu, F.-C., H.W. Shen, and Y.-J. Chou. 1999. Variation of roughness coefficients for Unsubmerged and submerged vegetation. *Journal of Hydraulic Engineering* 125: 934–942. doi:10.1061/(ASCE)0733-9429(1999)125:9(934).

Xue, B., M. Keming, Y. Liu, Z. Jieyu, and Z. Xiaolei. 2008. Differences of ecological functions inside and outside the wetland nature reserves in Sanjiang plain. *China. Acta Ecol. Sin.* 28: 620–626. doi:10.1016/S1872-2032(08)60028-1.

Zhang, K., H. Liu, Y. Li, H. Xu, J. Shen, J. Rhome, and T.J. Smith III. 2012. The role of mangroves in attenuating storm surges. *Estuarine, Coastal and Shelf Science* 102–103: 11–23. doi:10.1016/j.ecss.2012.02.021.